J Solid State Eletrochem (2004) 8: 435–441
DOI 10.1007/s10008-003-0460-2

ORIGINAL PAPER

Eimutis Juzeliũnas · Yu Pei Ma · John P. Wikswo

Remote sensing of aluminum alloy corrosion by SQUID magnetometry

Received: 28 May 2003 / Accepted: 19 September 2003 / Published online: 25 November 2003

Abstract Macroscopic magnetic fields were detected on corroding aluminum alloy (AA 2024) samples by SQUID magnetometry. The fields originated from corrosion reactions due to asymmetric sample geometry, electrolyte flow and differences in surface activity. Magnetic images were obtained by a SQUID magnetometer operating in liquid helium with a spatial resolution of approximately 1 mm. The measurements demonstrated SQUID capability for corrosion sensing across integrated media consisting of gaseous and solid dielectrics (air, plastics), an electronic conductor (aluminum alloy) and an ionic conductor (solution). The results show the potential of SQUID magnetometry for practical corrosion detection in restricted locations (''hidden'' corrosion) and in subjects where solution flow is applied.

Keywords Aluminum alloy · Corrosion · Hydrodynamic flow · Magnetometry · SQUID

Introduction

SQUID magnetometry has attracted considerable attention as a promising tool to evaluate nondestructively the corrosion and degradation of electrically conductive structures. The concepts of SQUID nondestructive evaluation (NDE) may be divided into several categories according to the origin of the measured magnetic fields: in situ electrochemical charge transfer reactions [1, 2, 3, 4, 5, 6, 7, 8, 9, 10, 11, 12, 13, 14], induced eddy currents [15, 16, 17, 18, 19] and piezomagnetism of ferromagnetic materials [20, 21].

The major advantage of magnetometric corrosion sensing lies in its unique ability to detect corrosion activity remotely across a dielectric medium, which is virtually impossible using conventional electrochemical techniques. This approach provides, therefore, an opportunity to detect subsurface (''hidden'') corrosion in restricted locations.

As a rule, corrosion has to be considered as a spatially localized phenomenon. The inhomogeneity of a corroding surface causes development of micro-galvanic cells, whose dimensions at the initial stages could be in the order of microns or even less. Therefore, in situ detection of a magnetically active corrosion area (corrosion pit, etc.) would demand a SQUID technique with a high spatial resolution. The SQUID microscopes, however, usually have a relatively modest spatial resolution (roughly 1 mm), although improvement is in progress. Baudenbacher et al. [22] have recently developed a SQUID microscope to image weak magnetic fields to measure various biomagnetic and paleomagnetic fields. They used submillimeter pickup coils from low-temperature superconducting niobium wire coupled to the input circuit of a SQUID and achieved a spatial resolution of 250 μm with a magnetic field sensitivity of 850 $fT/Hz^{-1/2}$.

Corrosion detection by conventional SQUID scanning techniques is possible, provided that the corroding surface generates macroscopic magnetic fields. These can appear due to differences in electrochemical potentials, which may be caused by numerous physicochemical factors. In this study, attention has been focused to induce large-scale magnetic fields by using asymmetric samples, hydrodynamic electrolyte flow and surfaces

Contribution to the 3rd Baltic Conference on Electrochemistry, GDAŃSK-SOBIESZEWO, 23–26 APRIL 2003.

Dedicated to the memory of Harry B. Mark, Jr. (February 28, 1934 – March 3rd, 2003)

E. Juzeliũnas (✉)
Institute of Chemistry,
A. Goštauto 9,
2600 Vilnius, Lithuania
E-mail: ejuzel@ktl.mii.lt

Y. P. Ma · J. P. Wikswo
Department of Physics and Astronomy,
Vanderbilt University,
VU Station B 351807,
Nashville, TN 37235, USA

with domains of different electrochemical activity. Our goal was to demonstrate the capability of SQUID magnetometry to detect electrochemical (corrosion) activity remotely and across a multiphase system, which consisted of dielectrics and both electronic and ionic conductors. Attempts were addressed to design systems which simulated, to a certain extent, a broad class of subjects of practical importance (subsurface corrosion in pipelines and aircraft structures, metal degradation beneath protective organic and conversion coatings, etc.).

Experimental

A high-resolution SQUID facility at Vanderbilt University was used, which was described in detail previously [14]. The SQUID magnetometer, operating in liquid helium (Tristan Technologies), had a three-axis vector gradiometer system with a noise-canceling reference SQUID. For each axis a first-order differential gradiometer used a pair of pickup coils (diameter 3 mm) separated vertically by a 30 mm baseline. The minimum operational distance between the z pickup coil and the Dewar outside (room temperature) was 2.5 mm. The SQUID was controlled by a modified QD 5000 (Quantum Design) electronics that provided external feedback on four channels. A magnetic shield with dimensions of 1 m×1.7 m×2 m consisted of two layers of Amumetal and two layers of aluminum, which provided the environment for the SQUID not higher than 12 $fT/Hz^{-1/2}$. A nonmagnetic, high-speed x-y scanning stage driven by two stepper motors was placed outside the magnetic shield. It provided repeatable scans with positioning accuracy less than 0.1 mm. The experimental setup is shown in Fig. 1.

Figure 2 shows the design of the corrosion cell used under no-flow conditions. The cell was sandwiched from a Plexiglas cell body, a rubber seal and a Plexiglas cover with an AA 2024 alloy sample underneath the cover. The scanning duration of the entire area was ca. 18 min. The starting point of the scanning and its direction is indicated on Fig. 2.

The U-shaped samples were prepared from a commercial 1.5-mm thick AA 2024 aluminum alloy plate (McMaster Carr). The surface treatment of the samples before each experiment included sandpapering (grades 320 and 600), cleaning with filter paper, rinsing with acetone, drying under ambient conditions, washing with distilled water and drying again.

In some experiments under solution flow the sample was not glued to the cover but placed inside the corrosion cell, as shown in Fig. 3. All sides of the specimen except the working one (which faced the solution) were isolated by epoxy resin. The cell was closed by two covers, viz. plastic and aluminum alloy AA 2024.

The assembled corrosion cell was connected to solution tubing and fixed on the x,y-stage in the magnetic shield (always in the same position). The distance between the SQUID Dewar and the sample at the bottom of the cell (Fig. 3) was ca. 12 mm, which included the air gap between the Dewar and the cell (2 mm), the AA 2024 and plastic covers (1.5 mm and 0.8 mm), the rubber seal (0.8 mm) and the solution (8 mm).

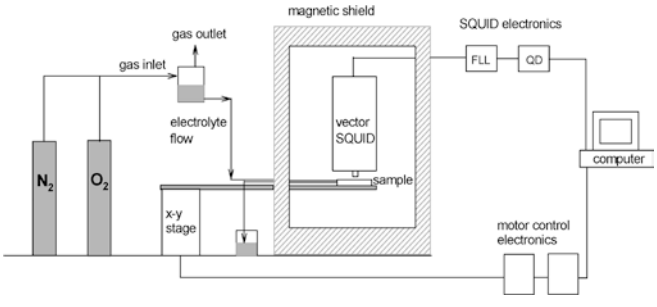

Fig. 1 Experimental setup of magnetic imaging system, solution and gas supply and corrosion cell inside a magnetic shield

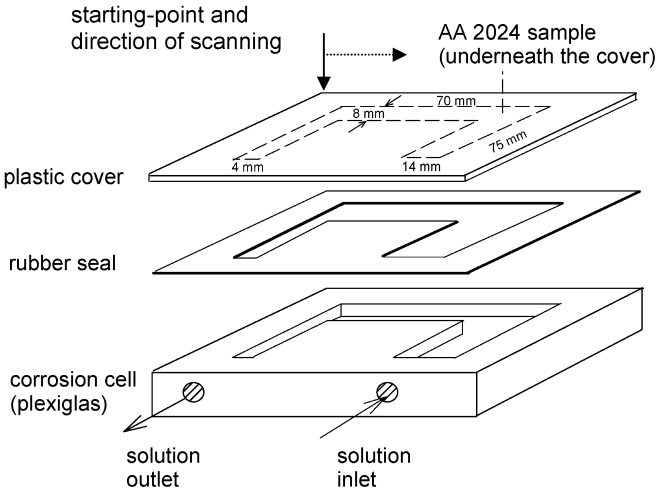

Fig. 2 The corrosion cell design with the AA 2024 sample underneath the cover used in the SQUID magnetometry experiments

The SQUID data were processed using a program which makes it possible to subtract one scanning result from another. Background magnetic field images (BG) were subtracted from the experimental data presented.

A 3.5% NaCl solution was used as the corrosion medium. The solution was prepared using a salt of analytical grade purity and distilled water. The experiments were performed at room temperature (20 ± 2 °C) and under natural aeration conditions (if not specified otherwise).

Results and discussion

The total magnetic activity of the scanned area was estimated by the spatially integrated magnetic activity method (SIMA, nT mm^2) [15]:

$$\mathrm{SIMA}(t_k, \Delta t) = \sum_{i}^{N_x} \sum_{j}^{N_y} \left[B_z\left(x_i, y_j, t_k, \Delta t\right) \right] \Delta x \Delta y \qquad (1)$$

where Δx and Δy represent the distance between two consecutive pixels in the corresponding scan direction. The SIMA calculation takes the summations over all the pixels in the magnetic image, i.e. this value is proportional to the net magnetic activity of the sample during the surface scanning time.

Figure 4 shows typical magnetic flux images (x, y, and z components) obtained over the corroding asymmetric sample (Fig. 2). The images imply an electronic current flow along the sample during the corrosion process. The origin of the current lies in the electromotive force, which appears due to a corrosion potential (E_{corr}) gradient along the sample. It is commonly known that E_{corr} depends upon various factors, which may affect the rate of both the anodic and cathodic partial reactions of the corrosion process. In our case, the

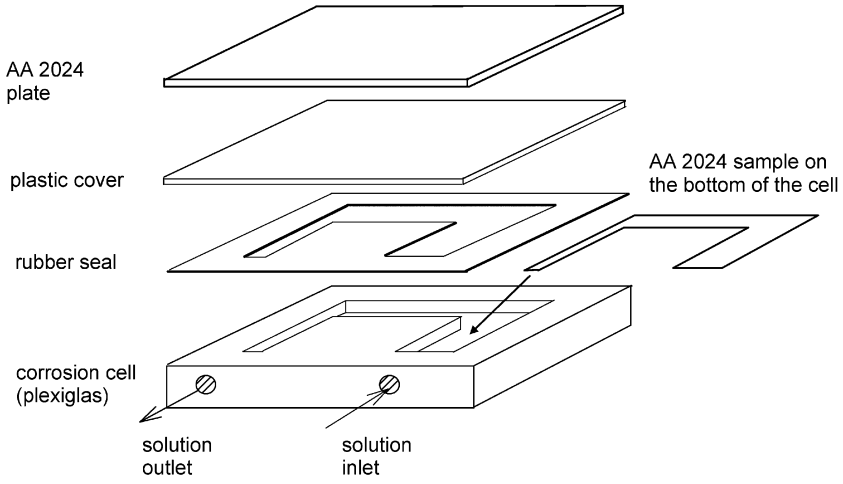

Fig. 3 Electrolyte flow cell design with the AA 2024 sample at the bottom of the cell, the rubber seal and the plastic and AA 2024 covers

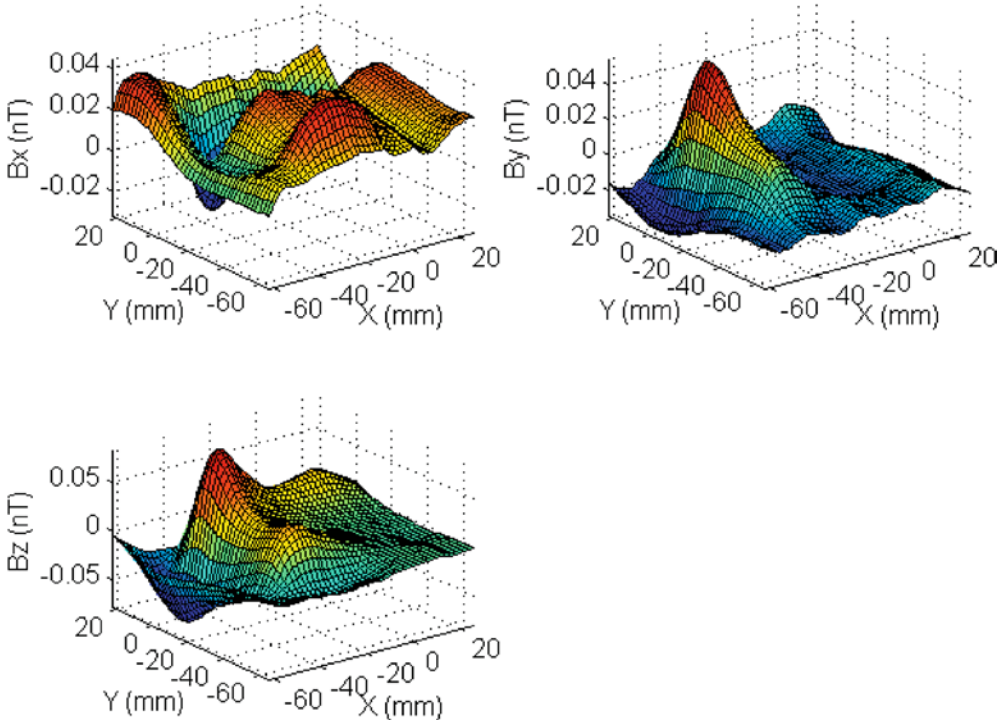

Fig. 4 Magnetic field images (x, y and z components) obtained for the sample in Fig. 2 in oxygen-saturated 3.5% NaCl solution under no-flow conditions. $SIMA_z = 186$ nT mm^2

corrosion potential on different sides of the sample will be somewhat different, primarily because of the different geometry and, consequently, different conditions of diffusion and convective transport of the oxidizing agent and corrosion products. As a result, the solution composition at the sample vicinity at the two ends of the sample will be different.

The current flow along the corroding sample and its direction was confirmed by the experiment in which an external d.c. current (0.1 mA) with the electron flow direction from the narrow side to the wide one was applied to the asymmetric sample (Fig. 5). It is obvious that the d.c. images show a resemblance to those obtained for the corroding sample (Fig. 4), with the main difference being that the applied electron current flows to the end of the sample, whereas the corrosion current diminishes closer to the ends.

The data imply that the anodic reaction of the corrosion process:

$$2Al + 3H_2O \rightarrow Al_2O_3 + 6H^+ + 6e^- \quad (2)$$

is somewhat promoted on the smaller side of the sample, whereas the cathodic reaction:

$$O_2 + 2H_2O + 4e^- \rightarrow 4OH^- \quad (3)$$

predominates on the larger side.

It should also be noted that corrosion activity in the static cell (Fig. 2) might change with time because of changes in the concentration of oxygen and the surface state of the corroding sample (the scanning time was ca. 18 min). Thus, the corrosion activity at the beginning and at the end of the scanning could be somewhat different.

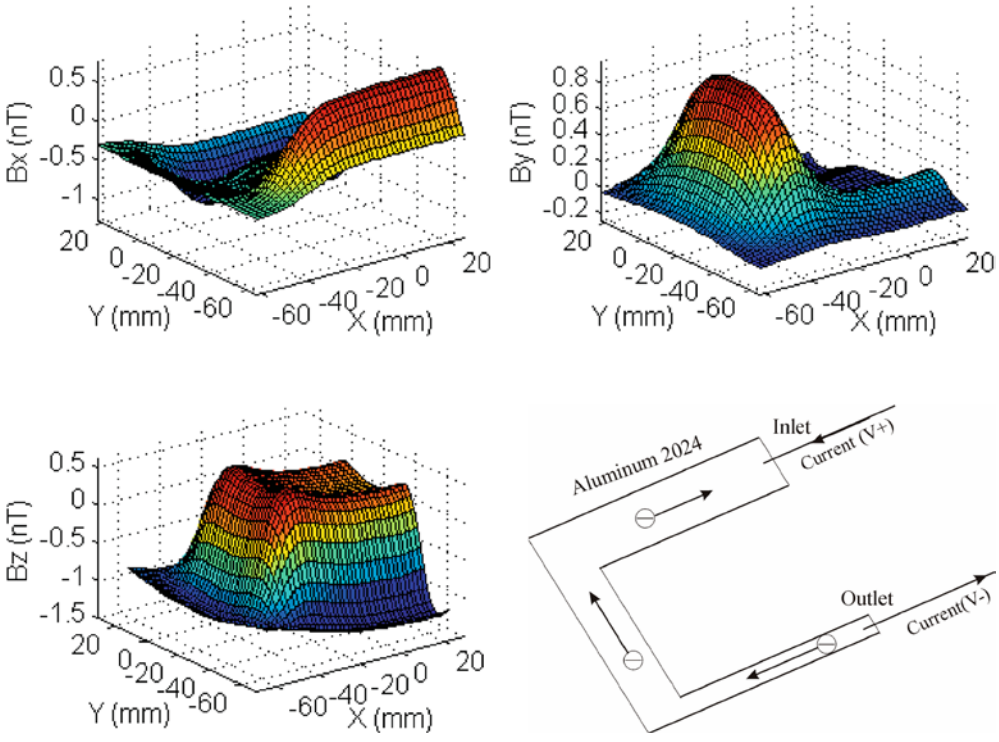

Fig. 5 Magnetic field images (x, y and z components) obtained when a d.c. current (0.1 mA) was passed through the sample (Fig. 2). The sample was mounted on the G-10 plate and the contacts were glued to the ends of the sample using silver paint. The current polarity is indicated on the *lower figure*

The magnetic sensitivity of the asymmetric sample to corrosion was also proven by experiments in deoxygenated, naturally aerated and oxygen-saturated solutions. It appeared that SIMA values increased with the solution corrosivity: $SIMA_{N2} \approx 110$ nT mm^2, $SIMA_{air} \approx 150$ nT mm^2 and $SIMA_{O2} \approx 190$ nT mm^2 (the magnetic field images in oxygen-free and open-to-air solutions are given elsewhere [14]). Thus, the magnetic activity responded to a corrosion rate change, viz. the higher corrosion rate, the higher the magnetic activity that was observed. At the same time, comparison of the EQCM data and the corresponding SIMA values indicated that some part of the corrosion was magnetically silent. This was evident from the ratios between the total mass change and the integrated magnetic activity in argon, air and oxygen-saturated solutions. {The microgravimetric data (EQCM) for the aluminum alloy corrosion rate dependence upon oxygen concentration were reported previously [14].}

Analogous experiments were performed in naturally aerated and oxygen-saturated solutions by using a sectional sample, i.e. the same sample as depicted in Fig. 2 was cut into 11 single sections with 1 mm isolating gaps. The magnetic activity of such a sample was approximately one order of magnitude lower compared to its monolithic counterpart. This indicated once again that electronic currents are induced by corrosion reactions on the asymmetric sample.

The total magnetic activity increased when a solution flow was applied (Fig. 6). The activity in a quiet solution was $SIMA_z = 186$ nT mm^2 (Fig. 4), whereas approximately twice as high a value ($SIMA_z = 332$ nT mm^2) was determined under solution flow ($v = 7.2$ mL s^{-1}). Qualitatively, the images for both quiet and flowing solutions are similar. The solution stream itself appeared to be more or less magnetically silent, as demonstrated in a hydrodynamic experiment without a metal sample (Fig. 7). The magnetic image does not indicate the geometry of the flow channels and the intrinsic magnetic activity of the electrolyte stream is significantly less than that resulting from a metal–solution interaction (Fig. 6).

The hydrodynamic magnetic field effects may originate from the currents induced by electrochemical potential gradients on the corroding surface. The cell construction allowed a solution stream with three different flow velocities. So, while the average velocity in Fig. 6 was $v = 7.2$ mL s^{-1}, the velocities in the channels were 12.6, 8.1 and 4.5 mL s^{-1} (in accordance with the channel width). The electrochemical (corrosion) potential is dependent upon numerous factors, such as chemical composition and pH in the vicinity of electrode, oxygen and corrosion product transport rate, thickness and physicochemical properties of the corrosion product layer, etc. In our experiments, the solution flow may affect all these factors and, therefore, flow-induced potential gradients may appear due to differences in flow velocity. The positive field effect in Fig. 6 means that under hydrodynamic conditions an additional current is superimposed (on that existing due to the sample asymmetric geometry), with the electron flow direction as indicated in Fig. 5. Related electrochemical processes are described by reactions (2) and (3), the first reaction being predominant at a higher flow velocity domain, while the second one is promoted at a lower velocity domain.

Another part of the experiments dealt with the sample at the bottom of the cell (Fig. 8). The cell was de-

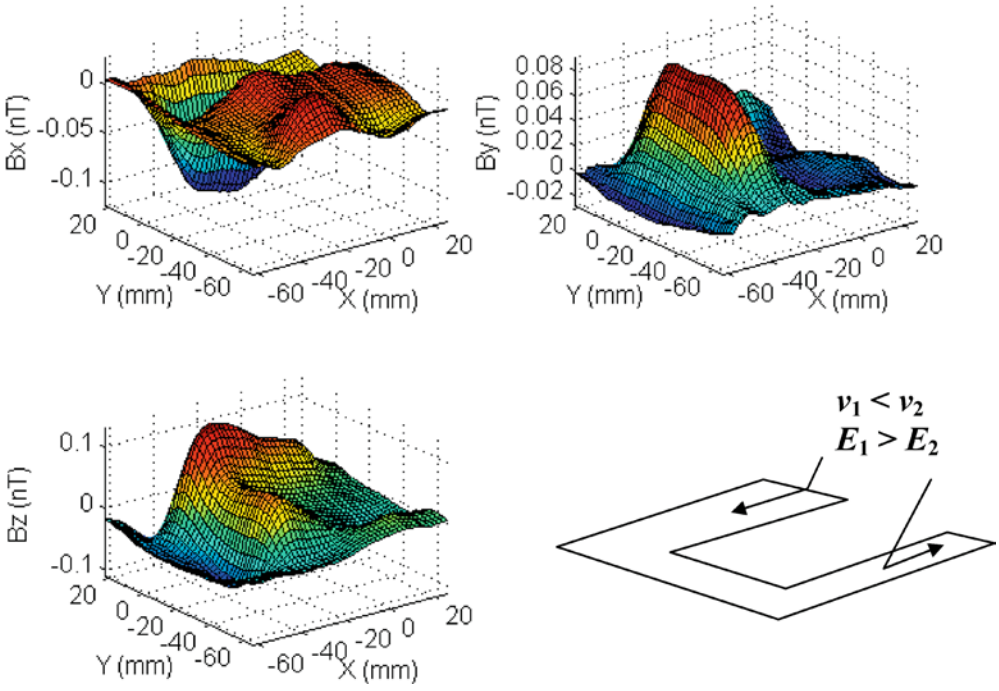

Fig. 6 Magnetic field images (x, y and z components) obtained for the sample in Fig. 2 in oxygen-saturated 3.5% NaCl solution under an electrolyte flow of 7.2 mL s^{-1}. $SIMA_z = 332$ nT mm^2. The cell design is given in Fig. 2

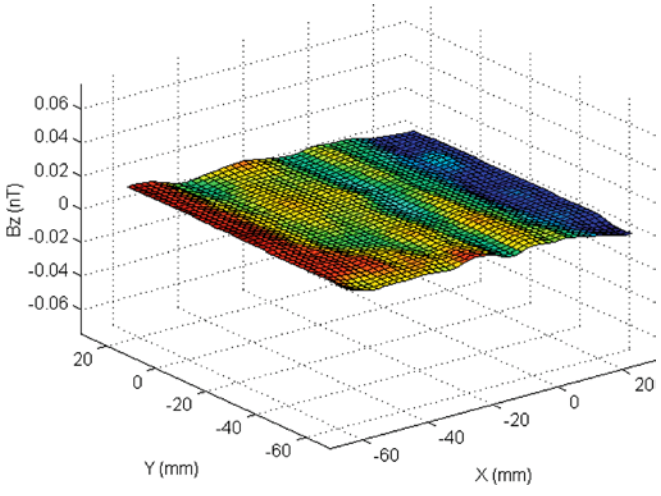

Fig. 7 Magnetic field image (B_z) over the cell without the metal sample (the cell is given in Fig. 2) under a flow of oxygen-saturated 3.5% NaCl solution ($v = 8.0$ mL s^{-1}). The data under no-flow conditions were subtracted from those obtained under electrolyte flow. $SIMA_z = 80$ nT mm^2

signed to demonstrate the SQUID capability of remote corrosion sensing (the distance between the sample and the Dewar was ca. 12 mm) across the integrated media, which included an ionic conductor (8 mm of NaCl solution). Significant magnetic activity was observed for an AA 2024 sample with non-isolated edges in 5 mM NaOH solution under electrolyte flow (Fig. 8c; $SIMA_{pH\ 11.5} = 1006$ nT mm^2). This was about five times as high as the activity in the analogous metal-free experiment (the data are not given in this paper). The magnetic activity was lower for the sample with isolated edges (Fig. 8b; SIMA = 519 nT mm^2), which implies that the edges are actively contributing to the magnetic field effects. The activity diminishes to SIMA = 106 nT mm^2 when the solution flow is terminated, which confirms once again the hydrodynamic generation of the magnetic fields. As discussed above, the effects under solution flow can be explained in terms of the hydrodynamic generation of an electromotive force due to the electrochemical (corrosion) potential gradient within the sample.

The magnetic activity of the specimen with two domains of different electrochemical activity is demonstrated in Fig. 9. The sample has three different surfaces: pristine mechanically treated (A), covered by an isolating film (B) and pre-corroded to 5 mM NaOH solution (C). [According to XPS analysis, the AA 2024 surface during exposure to 5 mM NaOH solution is enriched in copper and magnesium (Leinartas K, Sudavicius A, Juzeliunas E, unpublished data).] The image in Fig. 9 indicates clearly the magnetic activity of the sample in 3.5% NaCl solution. Such an experiment imitated, to a certain extent, a microgalvanic corrosion cell enlarged to macroscopic dimensions.

The macroscopic electronic currents are associated with the ionic ones which originate from ion emission by electrochemical reactions and associated hydrolysis of ions. Both electronic and ionic currents represent a closed contour, which extends in both metal and solution phases. This means that the electronic currents in the metal have an opposite direction to that of the ionic currents in the solution and, therefore, the magnetic fields induced by the electronic currents are oppositely directed to those induced by the ionic currents. However, both magnetic fields do not cancel each other because of different spatial distributions: the ionic currents are distributed in the large volume of the solution above or beneath the sample (depending on the cell design), while the electronic currents are localized within a much

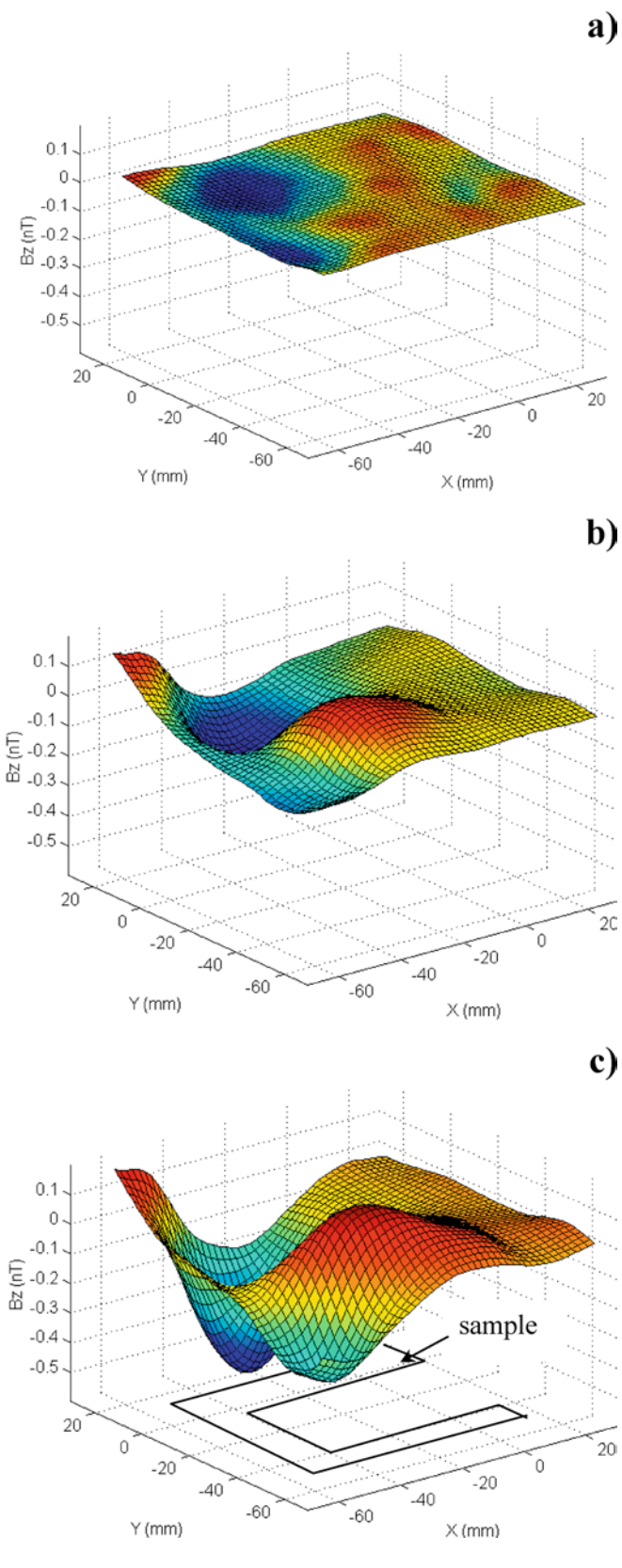

Fig. 8 Magnetic field images (B_z) for an AA 2024 sample in the cell given in Fig. 3 in quiet 5 mM NaOH (**a**) and under solution flow of $v = 1.3$ mL s^{-1} (**b** and **c**). The images **a** and **b** give data for the sample with isolated edges and underneath surface and the image **c** is for the sample without surface isolation. The image **a** was obtained immediately after **b** when the solution flow was terminated. Total magnetic activity (SIMA): **a**, 106 nT mm^2; **b**, 519 nT mm^2; **c**, 1006 nT mm^2

developing SQUID corrosion sensing techniques for practical applications.

Conclusions

Macro-scale magnetic fields were induced on aluminum alloy AA 2024 by breaking the symmetry, hydrodynamic electrolyte flow and differences in the surface electrochemical activity.

A U-shaped asymmetric sample exhibited magnetic activity during corrosion in NaCl solution. The field images implied an electronic current flow along the sample, the origin of which lies in the appearance of an electromotive force due to a corrosion potential gradient along the sample.

The magnetic activity of the U-shaped asymmetric sample increased when the solution flow was applied. The hydrodynamic induction of magnetic fields was explained in terms of the appearance of the currents within the sample owing to the corrosion potential gradients. The magnetic image of the liquid flow did not indicate the geometry of the flow channels and the intrinsic magnetic activity of the electrolyte flow was significantly less than that resulting from metal–solution interaction.

The sample with two domains of different electrochemical activity (pre-corroded vs. pristine) exhibited magnetic activity with a distinctive image, which

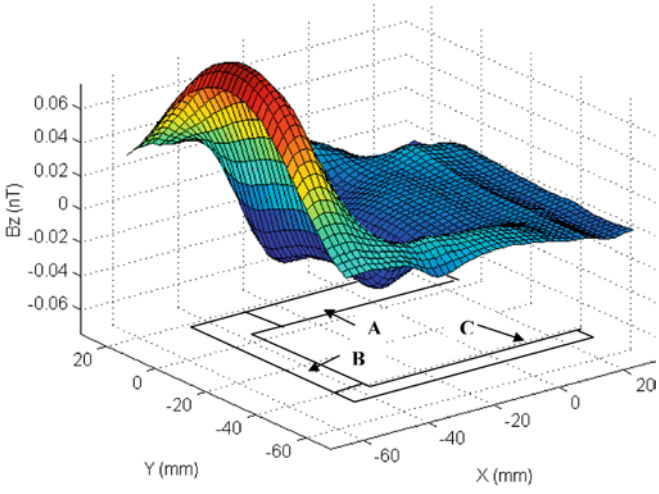

Fig. 9 Magnetic field image (B_z) for an AA 2024 sample with different activity domains: *A*, pristine mechanically abraded; *B*, covered with an isolating film; *C*, pre-exposed for 1 h 20 min to 5 mM NaOH. The cell design is given in Fig. 2

thinner sample. Nevertheless, one can expect that the ionic currents reduce the strength of the observed magnetic field compared to that produced by the electronic currents alone. These aspects are of importance when

reconstructed the sample geometry. The experiment supposes, in principle, the magnetic activity of micro-galvanic corrosion cells.

The macroscopic electronic currents are associated with ionic ones, both of them representing a closed contour, which extends in both the metal and solution phases. The ionic currents reduce the strength of the observed magnetic field compared to that produced by the electronic currents alone.

The SQUID magnetometer was demonstrated to be capable of remote sensing of a corroding surface across the multiphase system ''air–metal–plastic–solution''.

Acknowledgements E.J. acknowledges the Council for International Exchange of Scholars (Washington, DC) for a Fulbright research fellowship.

References

1. Bellingham JG, MacVicar MLA, Nisenoff M, Searson PC (1986) J Electrochem Soc 133:1753
2. Bellingham JG, MacVicar MLA, Nisenoff M (1987) IEEE Trans Magn 23:477
3. Misra M, Lordi S, MacVicar MLA (1991) IEEE Trans Magn 27:3245
4. Hibbs AD (1992) IEEE Trans Magn 28:2447
5. Li D, Ma YP, Flanagan WF, Lichter BD, Wikswo JP Jr (1995) J Min Met Mater Soc 47:36
6. Li D, Ma YP, Flanagan WF, Lichter BD, Wikswo JP Jr (1996) Corrosion 52:219
7. Li D, Ma YP, Flanagan WF, Lichter BD, Wikswo JP Jr (1997) Corrosion 53:93
8. Matthews R, Kumar S, Taussig DA, Whitecotton BR, Koch RH, Rozen JR, Woeltgens P (1997) Inst Phys Conf Ser 1–2:767
9. Richter H, Knecht A (1997) Materialprüfung 39:390
10. Andrieu C, Dalard F, Rameau JJ, Alcouffe F, Reboul MJ (1998) Mater Sci 33:3177
11. Juzeliunas E, Hinken JH (1999) J Electroanal Chem 477:171
12. Juzeliunas E, Samuleviciene M, Sudavicius A, Hinken JH (2000) Electrochem Solid State Lett 3:24
13. Yashiro H, Yoshizawa M, Kumagai N, Hinken JH (2002) J Electrochem Soc 149:B65.
14. Ma YP, Wikswo JP, Samuleviciene M, Leinartas K, Juzeliunas E (2002) J Phys Chem B 106:12549
15. Skennerton G, Abedi A, Kelly RG, Wikswo JP Jr (2000) J Corros Sci Eng 3/2 (athttp://www.cp.umist.ac.uk/JCSE/)
16. Hohmann R, Krause HJ, Soltner H, Zhang Y, Copetti CA, Bousack H, Braginski AI, Faley MI (1997) IEEE Trans Appl Superconduct 7:2860
17. Valentino M, Pepe G, Ruosi A, Peluso G (1998) J Phys IV 8:249
18. Valentino M, Ruosi A, Pepe G, Mollo V, D'Alto R, Peluso G (1999) Int J Mod Phys B 13:1117
19. Ruosi A, Pepe G, Peluso G (1999) IEEE Trans Appl Superconduct 9:3499
20. Claycomb JR, Tralshawala N, Miller JH (2000) IEEE Trans Magn 36:292
21. Weinstock H (1991) IEEE Trans Magn 27:3231
22. Baudenbacher F, Peters NT, Wikswo JP Jr (2002) Rev Sci Instrum 73:1247